Comparison of the University of California at Los Angeles Line-by-Line Equivalent Radiative Transfer Model and the Moderate-Resolution Transmission Model for accuracy assessment of the National Polar-Orbiting Operational Environmental Satellite System's Visible–Infrared Imager–Radiometer Suite cloud algorithms

S. C. Ou, K. N. Liou, Y. Takano, E. Wong, K. Hutchison, and T. Samec

To support the verification and implementation of the National Polar-Orbiting Operational Environmental Satellite System's Visible–Infrared Imaging–Radiometric Suite (VIIRS) algorithms used for inferring cloud environmental data records, an intercomparison effort has been carried out to assess the consistency between the simulated cloudy radiances–reflectances from the University of California at Los Angeles Line-by-Line Equivalent Radiative Transfer Model and those from the Moderate-Resolution Transmission Model (MODTRAN) with the 16 stream Discrete Ordinate Radiative Transfer Model (DISORT) incorporated. For typical ice and water cloud optical depths and particle sizes, we found discrepancies in the visible and near-infrared reflectances from the two models, which presumably are due to the difference in phase function (nonspherical versus Henyey–Greenstein), different numbers of phase function expansion terms (16 versus 200 terms), and different treatment of forward peak truncation in each model. Using the MODTRAN4, we also found substantial differences in the infrared radiances for optically thick clouds. These differences led to the discovery by MODTRAN4 developers of an inconsistency in the MODTRAN4–DISORT interface. MODTRAN4 developers corrected the inconsistency, which provided dramatic reductions in the differences between the two radiative transfer models. The comparison not only affects the prospective test plan for the VIIRS cloud algorithms but also should lead to improvements in future MODTRAN releases.

OCIS codes: 280.0280, 290.1090.

1. Introduction

The research presented in this paper was executed to assist in the verification and implementation of the National Polar-Orbiting Operational Environmental Satellite System's (NPOESS's) Visible–Infrared Imager–Radiometer Suite (VIIRS) algorithms used for inferring cloud environmental data records (EDRs) and to assess the accuracy of the simulated cloudy radiances–reflectances from the University of California at Los Angeles (UCLA) Line-by-Line Equivalent Radiative Transfer Model (LBLE). The VIIRS is being developed as part of the NPOESS platform to satisfy the operational requirements for the global remote sensing of atmospheric and surface properties.[1] One of the prime applications of VIIRS channels is the remote sensing of cloud EDRs, including optical thickness, particle size, cloud-top temperature, cloud cover–layers, and cloud height.[2] The solar and infrared (IR) algorithms for the retrieval of the two NPOESS cloud EDRs, i.e., the cloud optical thickness and effective particle size, require the use of a de-

S. C. Ou (ssou@atmos.ucla.edu), K. N. Liou, and Y. Takano are with the Department of Atmospheric and Oceanic Sciences, University of California, Los Angeles, 405 Hilgard Avenue, Los Angeles, California 90095-1565. E. Wong, K. Hutchison, and T. Samec are with Northrop-Grumman Space Technology, One Space Park, Redondo Beach, Los Angeles, California 90278.

Received 13 December 2004; revised manuscript received 8 April 2005; accepted 11 April 2005.

0003-6935/05/296274-11$15.00/0

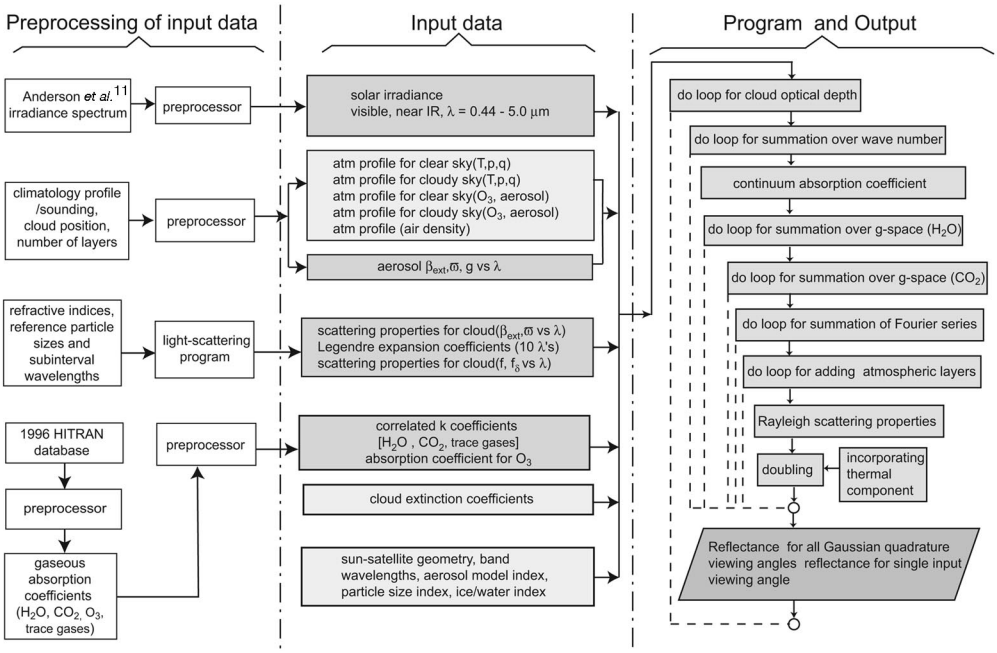

Fig. 1. Flow chart of the UCLA LBLE radiative transfer code.

tailed radiative transfer model. For this purpose the LBLE was developed specifically for simulating clear and cloudy reflectance–radiance to facilitate the development of and sensitivity analyses for cloud retrieval approaches that use the VIIRS.

To evaluate the performance of cloud algorithms with respect to cloud EDR specifications by the NPOESS Integrated Program Office,[3] it is planned that simulated reflectance–radiance fields will be generated by use of the Moderate-Resolution Transmission Model (MODTRAN) in conjunction with cloud scene data generated by the Cloud Scene Simulation Model and atmospheric sounding data from the National Centers for Environmental Prediction. The solar and viewing geometry will be sampled based on the three NPOESS orbit planes. To interpret the results from synthetic retrievals by using this data set, it is desirable to quantify and, it is hoped, to minimize the differences between the reflectance and the radiance produced by the two radiative transfer models before these tests are carried out.

For this purpose, we have compared visible and near-IR reflectances and IR radiances from the LBLE with those from the MODTRAN4 v1 (M1) and the MODTRAN4 v3rl (M3) with the Discrete Ordinate Radiative Transfer Model (DISORT).[4,5] To reduce the differences between visible and near-IR ice cloud reflectances from the two radiative transfer models, we utilize the user-defined hexagonal ice crystal phase functions[6] in the M3 code.

Using M1, we also found substantial differences in the IR radiances for optically thick clouds. These differences led to the identification by MODTRAN4 developers of an inconsistency in the MODTRAN4–DISORT interface. The MODTRAN4 team subsequently corrected the inconsistency, implemented the correction in the MODTRAN4 v4 (M4), and showed drastic reductions in the differences between the two radiative transfer models. In Section 2 we briefly describe the radiative transfer models and their built-in single-scattering parameters. In Section 3 we present results of the comparison. Finally, Section 4 contains a summary and recommendations for future research.

2. Single-Scattering Parameters Incorporated in the LBLE and the MODTRAN–DISORT

A. LBLE

The LBLE uses the adding–doubling method, including full Stokes parameters developed by Takano and Liou,[6] for vertically inhomgeneous atmospheres. Figure 1 shows a flow chart of the radiative transfer model developed for application to cloud remote sensing by use of VIIRS channel radiances. First we preprocess the spectral solar constant for VIIRS 0.67, 0.86, 1.24, 1.38, 1.61, 2.25, 3.70, 8.55, 10.76, and 12.01 μm channels, climatology or sounding profiles with the specification of cloud position and number of layers, and refractive indices and reference particle sizes for ice and water cloud particles. The gaseous absorption coefficients for these VIIRS bands are adopted from the 1996 HITRAN database[7] and are nearly the same as those from the updated 2000 HITRAN database.[8] The input parameters required for driving the LBLE are then generated by the preprocessors. These data include solar insolation, spectral band wave numbers of interest, solar and viewing zenith angles, relative azimuthal angle, spectral surface albedos and emissivities, atmospheric temperature and humidity, and aerosol profiles. Input cloud configuration parame-

ters include cloud phase, cloud base height (z_{cb}), cloud thickness (Δz), cloud optical depth (τ), and cloud effective particle size (r_e/D_e).

The LBLE offers the options of using the detailed solar irradiance data given by Thekaekara[9] (solar constant, 1353 W/m^2), Kneizys *et al.*[10] (solar constant, 1380 W/m^2), and Anderson *et al.*[11] (solar constant, 1375 W/m^2) averaged over appropriate spectral resolutions. The correlated-k coefficients for H_2O covering the spectral region of 2000–21,000 cm^{-1} (0.5–5 μm) are derived by following a numerical approach[12] in which efficient and accurate parameterizations for calculation of the pressure- and temperature-dependent absorption coefficients are developed based on theoretical values at 3 reference temperatures and 19 reference pressures. Absorption owing to O_3 and O_2 bands is also quantified in the model according to Beer's law.[13] In addition, we have compiled the single-scattering properties of six typical aerosol types provided by d'Almeida *et al.*[14] for incorporation into the LBLE. In the research reported here, we use the rural aerosol model with 23 km visibility at the surface, which is the same as the default aerosol model in the MODTRAN. At this point, the entire solar spectrum is divided into a total of 380 intervals, each of which is 50 cm^{-1} wide. For each spectral interval, the inverse of cumulative probability function $k(\gamma)$ is evaluated at 30 γ values, where $0 < \gamma < 1$. The resultant single-scattering parameters, cumulative k-distribution functions, and phase functions as well as auxiliary data were combined and built into the radiative transfer program.

We divided the model vertical domain into 51 layers ($\Delta p = 20$ hPa for each layer except for the bottom layer, where $\Delta p = 13$ hPa. The doubling procedures were applied to each layer, starting with an extremely thin layer with optical depth $\sim 10^{-8}$, to yield the layer reflection and transmission functions. Subsequently, we applied the adding procedures to the 51 layers to obtain the radiance at the top of atmosphere. For wavelengths from 3.5 to 5 μm we took into account the thermal emission contributions in the solar flux transfer by adding the emission part, $(1 - \varpi)\pi B_v(T)$, to the adding–doubling method in a manner described by Takano and Liou,[15] where ϖ is the single-scattering albedo and $B_v(T)$ is the Planck function for a given layer temperature T. We have compared visible, near-IR, and IR clear radiances from the LBLE with those from the MODTRAN.[16] Clear radiances differ by less than 10%, possibly because of the different treatment of multiple scattering in the two models.

Single-scattering parameters, which include asymmetry factor g, extinction coefficient β_e, and absorption coefficient $(1 - \varpi)\beta_e$ for ice clouds, are adapted from the geometric ray-tracing method, assuming randomly oriented hexagonal ice crystals.[15–19] The phase function values at discrete scattering angles for 0.67, 1.6, and 2.25 μm were computed from a 200 term Lengendre polynomial expansion of a hexagonal ice crystal phase function subject to the truncation of δ-function transmission (f_δ) and the diffraction (f) peaks. The phase function values for 3.7 and 10.8 μm were obtained from a 200 term Legendre polynomial

Table 1. Summary of Single-Scattering Properties Incorporated into LBLE, M1, M3, and M4

	Model		
Property	LBLE	M1	M3–M4
Ice cloud single-scattering parameters (ϖ, g, β_e)	From the geometric ray-tracing method, assuming randomly oriented hexagonal ice crystals	Same as LBLE (user defined)	Same as LBLE (user defined)
Ice cloud phase function for 0.67, 1.6, and 2.25 μm	200 term Legendre polynomial expansion of the hexagonal ice crystal phase function subject to the truncation of the δ-function transmission (f_δ) and the diffraction (f) peaks	H–G phase function at specified ϖ and g	Exact tabulation of hexagonal ice crystal phase function plus corresponding Legendre polynomial expansion coefficients; phase function subject to δ–M truncation
Ice cloud phase function for 3.7 and 10.8 μm	200 term Legendre polynomial expansion of the H–G phase function	H–G phase function at specified ϖ and g	H–G phase function at specific ϖ and g from the LBLE
Water cloud single-scattering parameters (ϖ, g, β_e)	From Mie theory (*cf.* VIIRS COT/EPS ATBD[a])	Same as LBLE (user defined)	Same as LBLE (user defined)
Water cloud phase function for 0.67, 1.6, 2.25, 3.7, and 10.8 μm	200 term Legendre polynomial expansion of the H–G phase function	H–G phase function at specified ϖ and g	Same as M1

[a]Ref. 16.

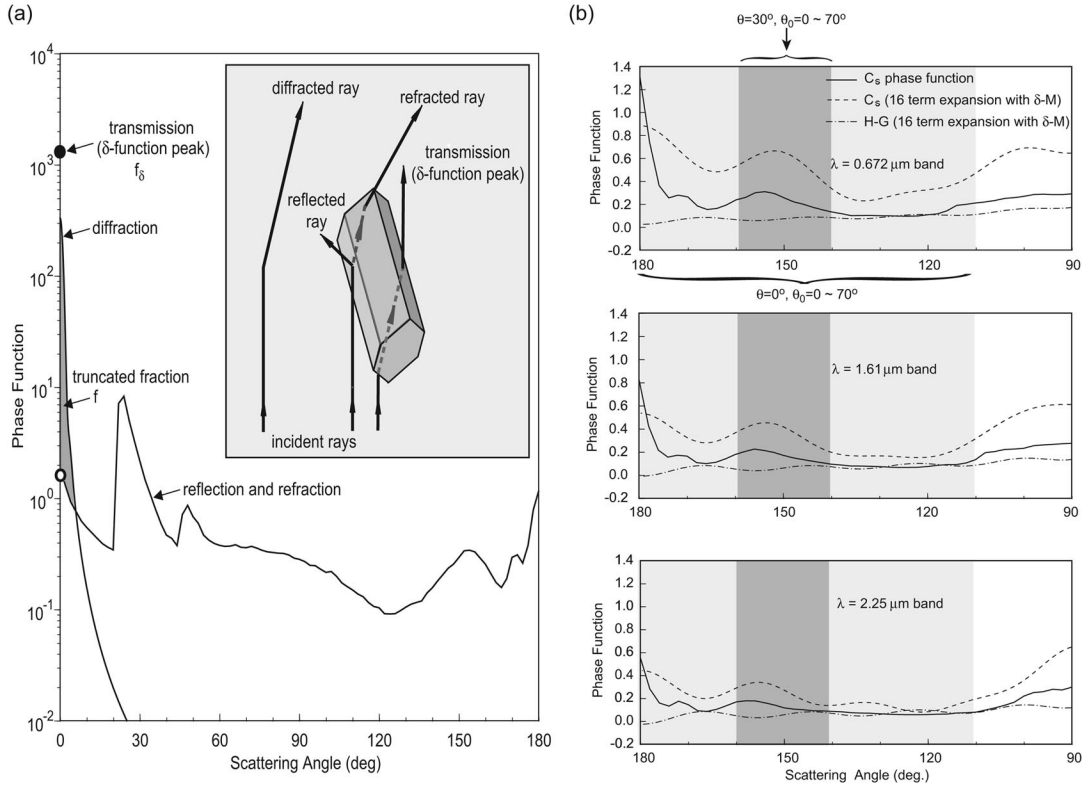

Fig. 2. (a) Schematic depiction of the components of the forward-scattering peak of a nonspherical ice crystal phase function, assuming random orientation. (b) Comparison of nonspherical ice crystal (C_s, D_e = 42 μm) phase function with a H–G phase function.

expansion of the Henyey–Greenstein (H–G) phase function. Traditionally, a phase function is expanded in Legendre polynomials in the form

$$\begin{aligned} P(\Theta) &= P(\mu,\ \phi;\ \mu',\ \phi') \\ &= \sum_{i=0}^{N} \varpi_l P_l\big[\mu\mu' + (1-\mu^2)^{1/2}(1-\mu'^2) \\ &\quad \times \cos(\phi' - \phi)\big] \\ &= \sum_{m=0}^{M} \sum_{l=m}^{N} \varpi_l^m P_l^m(\mu) P_l^m(\mu') \cos\, m(\phi' - \phi), \quad (1) \end{aligned}$$

where the number of terms N can be arbitrary for the adding method but, for the DISORT, which is included in the MODTRAN4, N must be equal to the number of discrete streams to maintain the orthogonality property.[20] To make the comparison of reflectances meaningful, we set the number of Gaussian quadrature points for the LBLE to be the same as the number of discrete streams for the MODTRAN–DISORT. The H–G phase function has a unique expansion form:

$$\begin{aligned} P_{\mathrm{HG}}(\cos\,\Theta) &= (1-g^2)/(1+g^2-2g\,\cos\,\Theta)^{3/2} \\ &= \sum_{t=0}^{N} (2l+1) g^l P_l(\cos\,\Theta). \quad (2) \end{aligned}$$

For water clouds, single-scattering parameters are calculated from Mie theory.[16] The phase function values for 0.67, 1.6, 2.25, 3.7, and 10.8 μm are determined based on a 200 term Legendre polynomial expansion of the H–G phase function. In principle, the Mie scattering phase function should have been used in both radiative transfer models. However, at this point, the H–G phase function is used in the LBLE for the purpose of achieving consistency with M1, into which the H–G phase function is built. In a future upgrade effort, a Mie scattering phase function will be used.

B. MODTRAN

The MODTRAN calculates atmospheric transmittance and radiance for frequencies ranging from 0 to 50,000 cm^{-1} at moderate spectral resolution, primarily 1 cm^{-1}.[21] In the most recent published version (M3), gaseous absorption is simulated by use of a band model approach with the option of adding the correlated-k method. Multiple scattering within clouds is simulated by the DISORT. Although a larger number (as many as 256) of streams is required for satisfactory computational accuracy, it is estimated that, for an extensive simulation effort such as the generation of global test data sets,[22] the optimal number of streams for speedy yet reasonably accurate calculation of reflectances and radiances is 16.[5]

Initially, we acquired only M1, into which the phase function is invariably built as the H–G phase function for both ice and water clouds and for all wavelengths. As the present research effort progressed, we were able to obtain M3, which permits

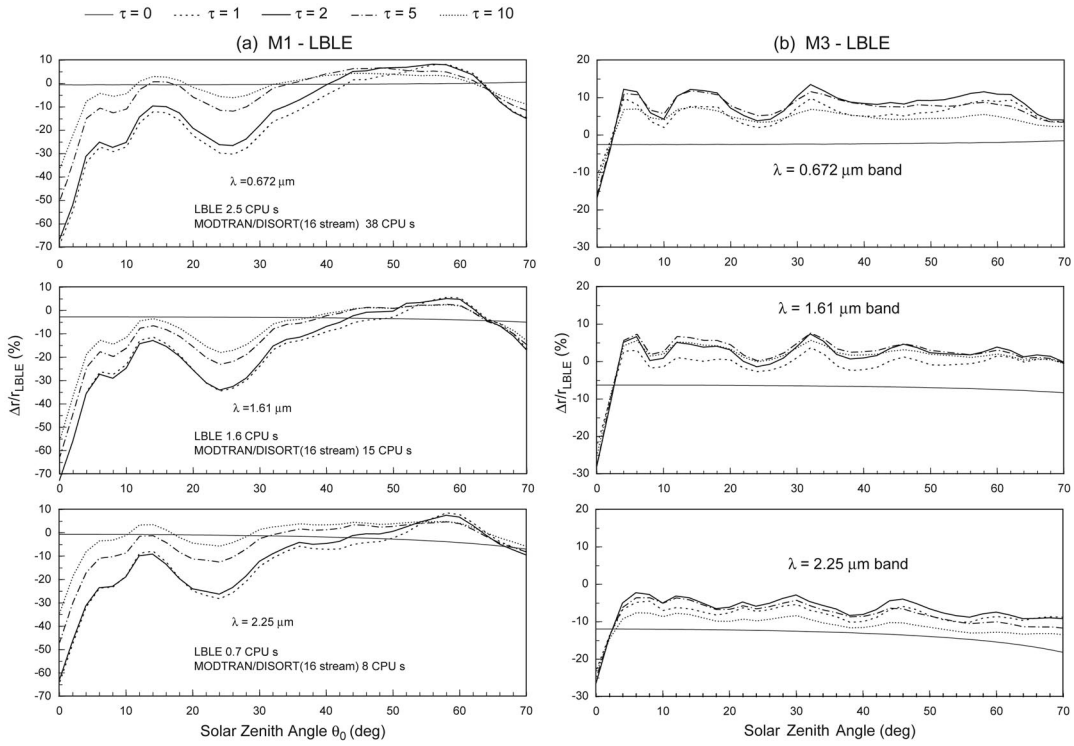

Fig. 3. Comparison of 0.672, 1.61, and 2.25 μm ice cloud reflectances as functions of solar zenith angles in terms of percentage differences ($\Delta r/r_{\mathrm{UCLA}}$) for ice cloud with $\theta = 0°$, $D_e = 42$ μm, and surface albedo of $A_s = 0.05$, where (a) $\Delta r = r_{\mathrm{M1}} - r_{\mathrm{UCLA}}$ and (b) $\Delta r = r_{\mathrm{M3}} - r_{\mathrm{UCLA}}$. Ranges of computational (CPU) time are 0.7–2.5 and 8–38 s for the LBLE and M1, respectively.

input of user-defined phase functions into the calculation. In the MODTRAN–DISORT, the input phase function is subject to δ–*M* truncation,[23] which chops off the strong forward-scattering peak that often occurs in the visible scattering of cloud particles. This truncation permits higher accuracy in the resultant expansion of the truncated phase function. Moreover, the M4 version, incorporating a corrected IR code in the DISORT, has been made available to Northrop-Grumman (see Subsection 3.B below).

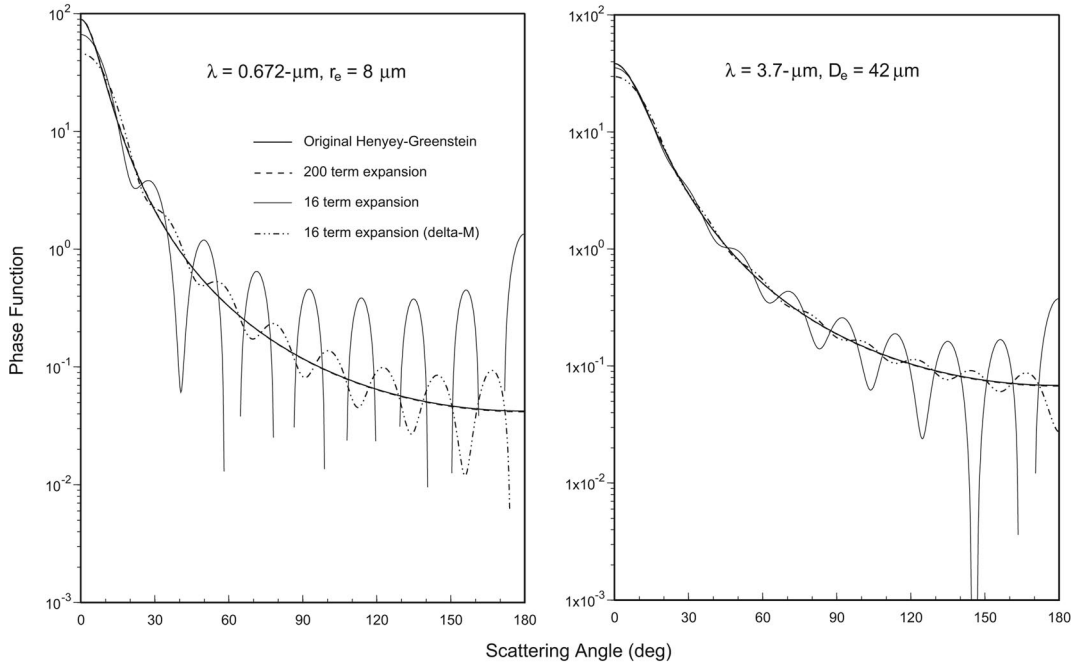

Fig. 4. Comparison of the algebraic and finite (16 and 200) term expanded H–G phase functions, as given in Eq. (2).

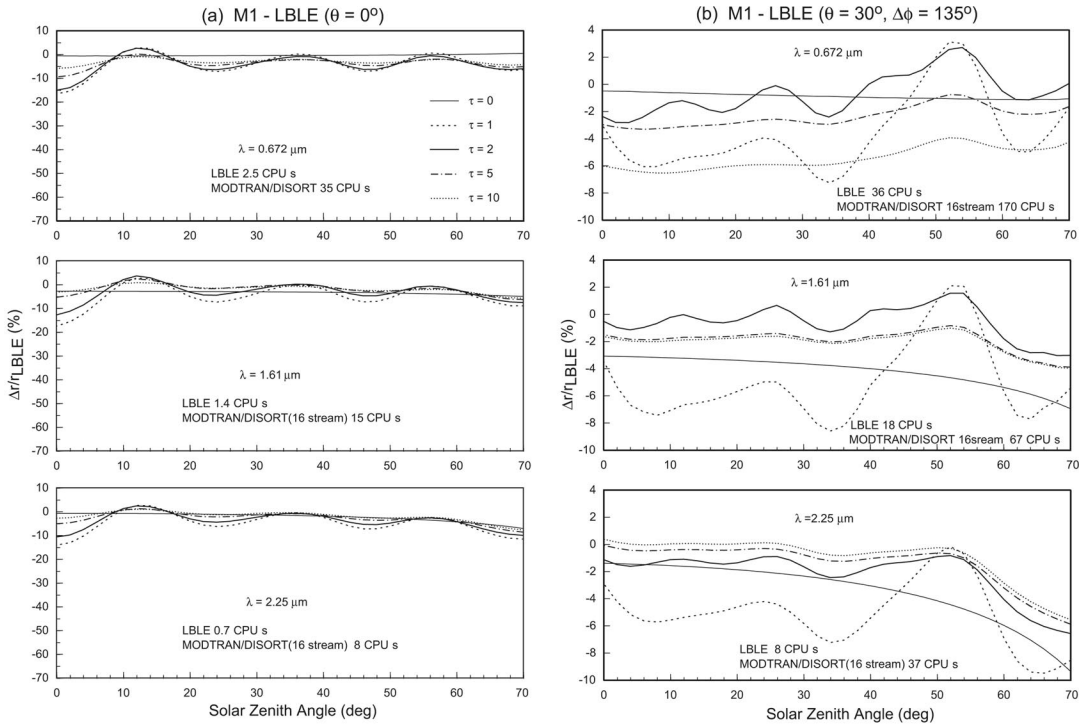

Fig. 5. Comparison of water cloud reflectances from the LBLE and M1 with $r_e = 8$ μm, $A_s = 0.05$, and the U.S. Standard Atmosphere. Ranges of CPU time are 0.7–2.5 and 8–35 s for LBLE and M3, respectively.

For M1, single-scattering parameters for ice clouds are user defined, and therefore they are the same as those used in the LBLE. The phase function used is a 16 term Legendre polynomial expansion of the H–G phase function. Single-scattering parameters for water clouds are the same as those used in the LBLE. The phase function is a Legendre polynomial expansion of the H–G phase function. For M4, single-scattering parameters for ice clouds are user defined, and therefore they are the same as those used in the LBLE. The phase function for visible and near-IR channels is a Legendre polynomial expansion of a user-defined hexagonal ice crystal phase function subject only to δ–*M* truncation. For thermal IR bands a Legendre polynomial expansion of the H–G phase function is used. For water clouds, single-scattering parameters are the same as those used in the LBLE, and the phase function is the same as in M1. Table 1 summarizes the single-scattering parameters incorporated into each model. The input Sun–satellite geometrical angles, atmospheric profiles, and cloud boundary and optical properties for the MODTRAN are the same as those specified for the LBLE.

3. Comparison of Reflectance–Radiance Results

A. Comparison of Solar Reflectance

Because visible and near-IR reflectance depends on the phase function, particularly for optically thin clouds, first we examine the comparison of various phase functions used in the models. As shown in the inset of Fig. 2(a), when light is scattered by polyhedral particles, such as hexagonal ice crystals, there is a δ-function transmission through parallel basal planes in the forward-scattering direction ($\theta = 0°$) in addition to a diffraction peak. To obtain a more-accurate Legendre polynomial expansion form of the phase function we must truncate both the δ-function transmission (f_δ) and the diffraction (f) peaks, as shown in Fig. 2(a). The MODTRAN considers only the truncation of the diffraction peak (f).

Figure 2(b) shows a comparison of the cirrostratus (C_s, $D_e = 42$ μm) phase functions, the 16 term expansion of the δ–*M* truncated C_s phase function, and the 16 term expansion of the δ–*M* truncated H–G phase function for 0.672, 1.61, and 2.25 μm channels. Because the Sun–satellite geometry corresponds mostly to backscattering and side-scattering situations, we show the comparison for scattering angle $90° < \Theta < 180°$, where shaded areas represent the range of solar zenith angles for satellite viewing zenith angles of 0° (nadir) and 30°. The 16 term expansion of both the δ–*M* truncated C_s and the H–G phase functions systematically deviates from the C_s phase function. These errors are caused by the inability of the 16 term expansion to represent properly the weaker forward peak after truncation and also by the normalization requirement, which forces errors in the forward direction to be offset by those in the backscattering direction.

Figure 3 shows a comparison of 0.672 (0.662–0.682) μm, 1.61 (1.54–1.64) μm, and 2.25 (2.225–2.275) μm reflectances as functions of solar zenith angles from the LBLE, M1, and M3 in terms of percentage differences ($\Delta r / r_{\mathrm{UCLA}}$) for ice cloud with $\theta = 0°$, $D_e = 42$ μm, and

Table 2. Comparison of 3.7 μm Top-of-Atmosphere Radiance[a] for Ice Cloud

Optical Depth	Model: LBLE R [(W/m^2)/sr]	M1 16 Stream ΔR [(W/m^2)/sr][b]	M1 16 Stream $\Delta R/R_{\mathrm{UCLA}}$ (%)	M4 16 Stream ΔR [(W/m^2)/sr][b]	M4 16 Stream $\Delta R/R_{\mathrm{UCLA}}$ (%)
0	4.5154×10^{-2}	-2.034×10^{-3}	−4.51	-0.2032×10^{-2}	−4.54
1	3.4250×10^{-2}	-3.211×10^{-4}	−0.94	-0.0565×10^{-2}	−1.65
2	2.5055×10^{-2}	2.642×10^{-3}	10.5	0.0434×10^{-2}	1.73
5	9.0692×10^{-3}	1.099×10^{-2}	12.1	1.2468×10^{-3}	13.75
10	2.1574×10^{-3}	1.525×10^{-2}	707	0.4949×10^{-3}	22.94
20	1.0509×10^{-3} (BT = 224 K)[c]	1.577×10^{-2} (BT = 267 K)[c]	1501	0.0404×10^{-3} (BT = 224.3 K)[c]	3.84
Planck function	1.0770×10^{-3} (T_c = 224 K)[d]				

[a] $\varepsilon_s = 0.95$, U.S. Standard Atmosphere, $D_e = 42$ μm, $\theta = 0°$, no aerosols.
[b] $\Delta R = R_{\mathrm{MODTRAN}} - R_{\mathrm{UCLA}}$.
[c] BT = $B_{3.7\ \mu\mathrm{m}}^{-1}(R)$.
[d] T_c is cloud temperature.

surface albedo of $A_s = 0.05$. The top-hat (step) instrument response function is used for all bands. The relationship between viewing and solar zenith angles θ and θ_0 and relative azimuthal angle $\Delta\phi$ was given in Fig. 6.1 of Ref. 13. The left- and right-hand sides of Fig. 3 display the percentage differences between the LBLE and M1 and between the LBLE and M3, respectively. The variation of differences exhibits a pattern that is similar to those shown in Fig. 2(b). For the comparison between the LBLE and M1 and for thin cloud, differences reach approximately 30%–70% in the backscattering direction ($\theta_0 = 0°$) but are mostly less than 10% in the side-scattering direction. This is so because the MODTRAN4's built-in H–G phase function deviates substantially from the C_s phase function in the backscattering directions but is closer to the C_s phase function in the side-scattering direction. Percentage differences are smaller for optically thicker clouds because of the smoothing effect of multiple scattering. Thus, we expect that, if M1 is used to generate synthetic radiance fields, synthetic retrievals based on the VIIRS lookup tables generated by the LBLE will produce unrealistic errors, particularly for solar zenith angles of less than 20°.

With the incorporation of user-defined nonspherical ice crystal phase functions, simulated LBLE visible and near-IR reflectances differ from M3 reflectances by ~10% for most of the solar zenith angles. In the backscattering direction, the difference (−10% to −30%) is much smaller than that from M1. For comparison purposes, the VIIRS-system-specified signal-to-noise ratios are 370/3300, 500/860, and 15/26 for 0.672, 1.61, and 2.25 μm bands, respectively.[1] The reason that there are still differences between the two models is that the MODTRAN–DISORT does not consider the truncation of the δ-function transmission peak. In the side-scattering direction the difference (~10%) is about the same as that from M1. Differences for reflectances are larger in the backscattering direction than

Table 3. Comparison of 10.8 μm Top-of-Atmosphere Radiance[a] for Ice Cloud

Optical Depth	Model: LBLE R [(W/m^2)/sr]	M1 16 Stream ΔR [(W/m^2)/sr][b]	M1 16 Stream $\Delta R/R_{\mathrm{UCLA}}$ (%)	M4 16 Stream ΔR [(W/m^2)/sr][b]	M4 16 Stream $\Delta R/R_{UCLA}$ (%)
0	7.8654	−0.0136	−0.17	−0.0138	−0.18
1	5.563	−0.0859	−1.54	−0.0771	−1.39
2	4.182	0.1515	3.62	−0.1105	−2.64
5	2.5797	0.8987	34.8	−0.0841	−3.26
10	2.1801	1.1984	55.0	−0.0353	−1.62
20	2.1354 (BT = 224 K)[c]	1.2245 (BT = 243 K)[c]	57.3	−0.0635 (BT = 223 K)[c]	−2.97
Planck function	2.1381 (T_c = 224 K)[d]				

[a] $\varepsilon_s' = 1.00$, U.S. Standard Atmosphere, $D_e = 42$ μm, $\theta = 0°$, no aerosols.
[b] $\Delta R = R_{\mathrm{MODTRAN}} - R_{\mathrm{UCLA}}$.
[c] BT = $B_{10.8\ \mu\mathrm{m}}^{-1}(R)$.
[d] T_c is cloud temperature.

Table 4. Comparison of 3.7 μm Top-of-Atmosphere Radiance[a] for Water Cloud

Optical Depth	Model: LBLE (R)	M1 16 Stream: ΔR ($\times 10^{-3}$)[b]	M1 16 Stream: $\Delta R/R_{\mathrm{UCLA}}$ (%)	M4 16 Stream: ΔR[b]	M4 16 Stream: $\Delta R/R_{\mathrm{UCLA}}$ (%)
0	0.045154	−2.03	−4.51	−0.002032	−4.54
1	0.040659	−1.006	−2.47	−0.001327	−3.26
2	0.029044	5.225	18.0	−0.000046	−0.16
5	0.024408	8.335	34.2	0.000089	0.37
10	0.022069	9.790	44.4	0.000003	0.02
20	0.021362	9.999	46.8	−0.000125	−0.58
	(BT = 272 K)[c]	(BT = 279 K)[c]		(BT = 272 K)[c]	
Planck function	0.025588 (T_c = 275.5 K)[d]				

[a] ε_s = 0.95, U.S. Standard Atmosphere, r_e = 8 μm, θ = 0°, no aerosols.
[b] $\Delta R = R_{\mathrm{MODTRAN}} - R_{\mathrm{UCLA}}$.
[c] BT = $B_{3.7\ \mu\mathrm{m}}^{-1}(R)$.
[d] T_c is cloud temperature.

in the side-scattering direction because of the inability of the finite 16 term expansion to simulate the backscattering peak. Because of the reduction of differences, it is expected that synthetic retrieval with an M3–16 stream DISORT with user-input phase functions will produce much smaller errors than use of M1 alone, and the retrieval accuracy would be closer to NPOESS EDR threshold requirements.

For water cloud, both models use single-scattering parameters derived from Mie scattering theory and the H–G phase function. However, the numbers of expansion terms in the phase function are different. Figure 4 shows a comparison of the algebraic and finite (16 and 200) term expanded H–G phase functions, as given in Eq. (2). The H–G phase functions are based on the asymmetry factors for a water-cloud

Table 5. Comparison of 10.8 μm Top-of-Atmosphere Radiance[a] for Water Cloud

Optical Depth	Model: LBLE (R)	M1 16 Stream: ΔR[b]	M1 16 Stream: $\Delta R/R_{\mathrm{UCLA}}$ (%)	M4 16 Stream: ΔR[b]	M4 16 Stream: $\Delta R/R_{\mathrm{UCLA}}$ (%)
0	7.8654	−0.0136	−0.17	−0.0138	−0.17
1	7.4265	−0.0397	−0.53	−0.0547	−0.74
2	6.7583	0.1694	2.51	−0.0644	−0.95
5	6.5474	0.3201	4.89	−0.0582	−0.89
10	6.4429	0.4023	6.24	−0.0580	−0.90
20	6.3977	0.4319	6.75	−0.0572	−0.89
	(BT = 275 K)[c]	(BT = 279 K)[c]		(BT = 275 K)[c]	
Planck function	6.4696 (T_c = 276 K)[d]				

[a] ε_s = 1.00, U.S. Standard Atmosphere, r_e = 8 μm, θ = 0°, no aerosols.
[b] $\Delta R = R_{\mathrm{MODTRAN}} - R_{\mathrm{UCLA}}$.
[c] BT = $B_{10.8\ \mu\mathrm{m}}^{-1}(R)$.
[d] T_c is cloud temperature.

Table 6. Percentage Difference [$\Delta R/R_{\mathrm{UCLA}}$(%)][a] of 3.7 μm Top-of-Atmosphere Radiance for Ice Cloud

Optical Depth	Particle Size, D_e (μm): 24	30	75	90	124
1	3.03	2.84	1.04	1.04	1.12
2	7.12	6.79	2.28	2.00	2.17
5	20.96	20.55	5.84	3.65	3.84
10	36.36	33.58	5.75	2.06	1.85
20	13.60	8.99	−0.77	−1.41	−1.57

[a] $\Delta R = R_{\mathrm{MODTRAN}} - R_{\mathrm{UCLA}}$.

Table 7. Percentage Difference [$\Delta R/R_{UCLA}(\%)$][a] of 10.8 μm Top-of-Atmosphere Radiance for Ice Cloud

Optical Depth	Particle Size, D_e (μm)				
	24	30	75	90	124
1	−1.67	−1.63	−0.85	−0.47	1.54
2	−3.13	−3.08	−1.54	−0.81	2.45
5	−3.67	−3.66	−2.07	−1.23	1.79
10	−1.78	−1.76	−1.21	−0.95	−0.25
20	−1.93	−1.91	−1.5	−1.37	−1.25

[a] $\Delta R = R_{MODTRAN} - R_{UCLA}$.

modified gamma size distribution with $r_e = 8$ μm for the 0.672 μm band and on the C_s distribution for the 3.7 μm bands. In both cases the 200 term Legendre expansion matches the algebraic H–G phase function almost exactly. However, the 16 term Legendre expansion oscillates above and below the algebraic H–G phase function.

Figure 5 shows a comparison of reflectances from the LBLE and M1 with $r_e = 8$ μm, $A_s = 0.05$, and the U.S. Standard Atmosphere. The left- and right-hand sides are for $\theta = 0°$, 30°, respectively. Because the MODTRAN4's 16 term expansions show a deviation from the 200 term expansion that is almost identical to the algebraic form of the H–G phase function, simulated reflectances from the two models differ, with the bulk of the differences near 10% and the maximum difference reaching 20%. These percentage differences are smaller than for ice cloud. Moreover, the pattern of oscillation of the magnitude of differences corresponds to the oscillation pattern of the 16 term phase function expansion between scattering angles of 90° and 180°. We estimate that retrievals that use MODTRAN4 simulated reflectances and VIIRS lookup tables (from the LBLE) will produce errors that are close to NPOESS EDR threshold requirements.[22]

Figures 3 and 5 also show comparisons of CPU time. For all spectral bands and for both ice and water cloud, the LBLE is at least ten times faster than the MODTRAN in the computation of nadir reflectance. This apparent efficiency of the LBLE can be attributed to the lower spectral resolution used in the model. However, for an off-nadir angle the LBLE is approximately five times faster than the MODTRAN. The reduction of efficiency for the off-nadir angle is due to the need to consider the azimuthal dependence of the bidirectional reflectance. It would be more computationally efficient if the LBLE were used to generate synthetic fields. However, the advantage of using the MODTRAN is that its program for computing clear radiances is more comprehensive than that of the LBLE.

B. Comparison of Infrared Radiance

Tables 2–5 show comparisons of 3.7 (3.66–3.84) μm and 10.8 (10.3–11.3) μm top-of-atmosphere (TOA) radiance for ice and water clouds from the LBLE, M1,

Table 8. Percentage Difference [$\Delta R/R_{UCLA}(\%)$][a] of 3.7 μm Top-of-Atmosphere Radiance for Water Cloud

Optical Depth	Particle Size, D_e (μm)							
	2	3	4	6	12	16	24	30
1	−0.24	−0.66	−0.70	−0.10	−0.84	−0.89	−0.88	−0.86
2	2.94	0.88	0.60	2.03	−0.95	−1.29	−1.40	−1.41
5	5.04	1.92	1.26	2.16	−1.19	−1.61	−1.80	−1.84
10	5.82	2.20	1.23	1.52	−1.50	−1.90	−2.14	−2.23
20	4.82	1.48	0.53	0.80	−1.99	−2.35	−2.54	−2.59

[a] $\Delta R = R_{MODTRAN} - R_{UCLA}$.

Table 9. Percentage Difference [$\Delta R/R_{UCLA}(\%)$][a] of 10.8 μm Top-of-Atmosphere Radiance for Water Cloud

Optical Depth	Particle Size, D_e (μm)							
	2	3	4	6	12	16	24	30
1	−0.26	−0.26	−0.29	−0.48	−0.80	−0.98	−0.13	−0.66
2	0.35	0.27	0.10	−0.43	−1.06	−1.22	−0.33	−0.70
5	0.62	0.40	0.14	−0.43	−0.97	−1.08	−0.65	−0.67
10	0.63	0.26	−0.02	−0.50	−0.98	−1.08	−0.87	−0.72
20	0.40	0.07	−0.15	−0.55	−0.94	−1.01	−0.89	−0.67

[a] $\Delta R = R_{MODTRAN} - R_{UCLA}$.

and M4. No solar component was added to the 3.7 μm radiance. To focus our comparison on the effects of cloud only, we chose not to include aerosol effects in the computations. For ice cloud (Tables 2 and 3), D_e = 42 μm, and, for water cloud (Tables 4 and 5), r_e = 8 μm. The difference in 3.7 μm clear radiances shown in Tables 2 and 4 is due to minor differences in the gas absorption parameterizations in both models. For example, the MODTRAN uses a combination of band model and the correlated-k distribution method, whereas the LBLE uses the correlated-k distribution method but with a different manner of binning the absorption coefficient spectrum. Moreover, the MODTRAN uses a much smaller spectral interval ($\Delta\nu$ = 1 cm^{-1}) than the UCLA LBLE ($\Delta\nu$ = 50 cm^{-1}).

There are significant differences between simulated radiances from the LBLE and the M1 16 stream models, particularly for large optical depth. The percentage differences increase with optical depth and are larger for the 3.7 μm channel than for the 10.8 μm channel. To investigate the cause of this difference, we employ the physical principle of thermal radiative emission. For optically thick cloud, which can be assumed to be thermally black, given that the scattering effects are small, it is well accepted that the radiation emitted by the cloud should be close to the Planck function of cloud-top temperature. To investigate whether thick-cloud radiances meet this requirement, we give brightness temperatures for ice and water cloud of optical depth 20 in parentheses along with the cloud temperature and associated Planck function values. It is obvious that the thick-cloud radiances from the LBLE are closer to the Planck function of cloud-top temperature than are those from M1.

As noted above, these differences prompted the MODTRAN4 developers to identify and correct an inconsistency in the MODTRAN4–DISORT interface, now fully implemented in M4. Tables 2–5 show that the differences between the LBLE and the MODTRAN4 are drastically reduced. However, for some unknown reasons, differences in the 3.7 μm radiance for ice clouds of optical depths 5 and 10 are still more than 10%. For comparison, the VIIRS-system-specified $NE\Delta T$s (noise equivalent delta temperatures) are 0.13–0.22 and 0.02–0.03 for the 3.7 and 10.8 μm bands, respectively.[1] Tables 6–9 then show the percentage differences of 3.7 and 10.8 μm TOA radiance for ice and water clouds from the LBLE and the MODTRAN4 for other particle sizes than those listed in Tables 2–5. The differences are no more than 6%, except those in the 3.7 μm radiance for ice cloud of optical depths 5 and 10 and D_e = 24, 30 μm. With these decreased differences, it is anticipated that the synthetic retrievals that use radiances generated by M4 will still produce results with accuracy that is close to NPOESS EDR specifications.

4. Summary and Recommended Future Research

To support the verification and implementation of VIIRS cloud EDR algorithms, we compared visible and near-IR reflectances and IR radiances generated from the LBLE and the MODTRAN for assessment of the consistency between the simulated cloudy radiances–reflectances from the two models. For typical ice and water cloud optical depths and particle sizes, we found discrepancies in the visible and near-IR reflectances in the two models that presumably are due to the difference in phase function (nonspherical versus Henyey–Greenstein), different numbers of phase function expansion terms (16 versus 200), and different treatment of forward peak truncation in each model. However, we expect that synthetic retrievals that use reflectance–radiance fields generated by the most recent version of the MODTRAN will produce an accuracy that is close to the NPOESS cloud EDR threshold requirements. For future upgrading efforts, to further reduce the differences in reflectances for ice clouds we shall work toward the development of a modified δ-function transmission forward-peak truncation scheme to be incorporated into MODTRAN coding.

Using M1, we also found substantial differences in IR radiance for optically thick clouds. These differences, caused by the inconsistency in the MODTRAN–DISORT interface for thick clouds, were drastically reduced to a few percent after the inconsistency was corrected in M4. The reduction in differences in radiance is expected to yield a synthetic retrieval accuracy close to the system specification. However, we still need to investigate the discrepancy in IR radiance for ice clouds with optical depths of 5 and 10 and D_e of 24–42 μm.

To sum up, the comparison study reported in this paper has led to an enhancement and a correction of the MODTRAN4, which should be of benefit to the MODTRAN user community. This study has also helped shape the prospective test plan for the testing of VIIRS cloud algorithms. To further enhance the performance of the MODTRAN in the long run, we believe that one possible approach would be to offer the adding–doubling method that is currently being used in the LBLE and other radiative transfer models as an alternative to the DISORT. The advantages of the adding–doubling method are that the phase function expansion can be made more exact, the computation can be more efficient, and the method is always numerically stable. By maintaining both options for the MODTRAN, the user community would be able to assess relative comparisons and cross validation, as well as historic compatibility.

The research reported here has been supported by Northrop-Grumman Space Technology through contracts 95031DDM3S and 97904DDM3S. The authors acknowledge the timely efforts of the MODTRAN4 developers, namely, A. Berk, Spectral Sciences, Inc., Burlington, Massachusetts; G. Anderson, U.S. Air Force Research Laboratory, Hanscom Air Force Base, Massachusetts; and E. Shettle, Naval Research Laboratory, Washington, D.C., in rapidly addressing the specific inconsistency in the MODTRAN4–DISORT interface.

References

1. C. Welsh, H. Swenson, S. A. Cota, F. DeLuccia, J. M. Haas, C. F. Schueler, R. M. Durham, J. E. Clement, and P. E. Ardanuy, "VIIRS (Visible Infrared Imager Radiometer Suite): a next-generation operational environmental sensor for NPOESS," presented at the International Geoscience and Remote Sensing Symposium (IGARSS), Sydney, Australia, 8–14 July 2001.
2. S. C. Ou, Y. Takano, K. N. Liou, G. J. Higgins, A. George, and R. Slonaker, "Remote sensing of cirrus cloud optical thickness and effective size for the National Polar-orbiting Operational Environmental Satellite System Visible–Infrared Imager Radiometer Suite: sensitivity to instrument noise and uncertainties in environmental parameters," Appl. Opt. **42,** 7202–7214 2003.
3. Associate Directorate for Acquisition NPOESS Integrated Program Office, "Visible/Infrared Imager/Radiometer Suite (VIIRS) Sensor Requirements Document (SRD) for National Polar-Orbiting Operational Environmental Satellite System (NPOESS) Spacecraft and Sensors," Version-2, Rev. a (NPOESS Integrated Program Office, Silver Spring, Md., 2000).
4. K. Stamnes, S.-C. Tsay, W. J. Wiscombe, and K. Jayaweera, "Numerically stable algorithm for discrete-ordinate-method radiative transfer in multiple scattering and emitting layered media," Appl. Opt. **27,** 2502–2509 (1988).
5. K. Stamnes, S.-C. Tsay, W. J. Wiscombe, and I. Laszlo, "DISTORT, a general purpose FORTRAN program for discrete-ordinate-method radiative transfer in scattering and emitting layered media: documentation of methodology," Rep. available from ftp://climatel.gsfc.nasa.gov/wiscombe/ (2000).
6. Y. Takano and K. N. Liou, "Radiative transfer in cirrus clouds. I. Single-scattering and optical properties of hexagonal ice crystals; II. Theory and computation of multiple scattering in an anisotropic medium," J. Atmos. Sci. **46,** 3–36 (1989).
7. L. S. Rothman and 31 additional authors, "The HITRAN molecular spectroscopic database and HAWKS (HITRAN Atmospheric Workstations): 1996 Ed.," J. Quant. Spectrosc. Radiat. Transfer **60,** 665–710 (1998).
8. L. S. Rothman and 31 additional authors, "THE HITRAN molecular spectroscopic database: edition of 2000 including updates through 2001," J. Quant Spectrosc. Radiat. Transfer **82,** 5–44 (2003).
9. M. P. Thekaekara, "Solar irradiance: total and spectral and its possible variation," Appl. Opt. **15,** 915–920 (1976).
10. F. X. Kneizys, E. P. Shettle, L. W. Abreu, J. H. Chettwynd, G. P. Anderson, W. O. Gallery, J. E. A. Selby, and S. A. Clough, "User guide to LOWTRAN 7" (U.S. Air Force Geophysics Laboratory, 1988).
11. G. P. Anderson, R. H. Picard, and J. H. Chetwynd, "Proceedings of the 17th Annual Review Conference on Atmospheric Transmission Models," Spec. Rep. 274 (Phillips Laboratory/Geophysics Directorate, Hanscom Air Force Base, 1995).
12. Q. Fu and K. N. Liou, "On the correlated *k*-distribution method for radiative transfer in nonhomogeneous atmospheres," J. Atmos. Sci. **49,** 2139–2156 (1992).
13. K. N. Liou, *An Introduction to Atmospheric Radiation*, 2nd ed., Vol. 84 of Academic International Geophysics Series (Academic, 2002).
14. G. A. d'Almeida, P. Koepke, and E. P. Shettle, *Atmospheric Aerosols, Global Climatology and Radiative Characteristics* (Deepak Publishing, 1991).
15. Y. Takano and K. N. Liou, "Transfer of polarized infrared radiation in optically anisotropic media: application to horizontally oriented ice crystals," J. Opt. Soc. Am. A **10,** 1243–1256 (1993).
16. S. C. Ou, K. N. Liou, Y. Takano, G. J. Higgins, A. George, and R. Slonaker, "VIIRS cloud effective particle size and cloud optical depth algorithm theoretical basis document," Algorithm Theoretical Basis Document, Version 5, Rev. 1 (Raytheon, Lanham, Md., 2002).
17. Y. Takano and K. N. Liou, "Radiative transfer in cirrus clouds. III. Light scattering by irregular ice crystals," J. Atmos. Sci. **52,** 818–837 (1995).
18. Y. Takano, K. N. Liou, and P. Minnis, "Effects of small ice crystals on cirrus infrared radiative properties," J. Atmos. Sci. **49,** 1487–1493 (1992).
19. K. N. Liou and Y. Takano, "Light scattering by nonspherical particles: remote sensing and climatic implications," Atmos. Res. **31,** 271–298 (1994).
20. S. Chandrasekhar, *Radiative Transfer* (Oxford U. Press, 1950).
21. A. Berk, L. S. Bernstein, and D. C. Robertson, "MODTRAN: A Moderate Resolution Model for LOWTRAN7," Rep. GL-TR-89-0122 (U.S. Air Force Geophysics Laboratory, 1989), pp. 1–38.
22. V. Grano, T. Scalione, P. Emch, H. Agraveante, B. Hauss, J. Jackson, S. Mills, T. Samec, and M. Shoucri, "End-to-end performance assessment of the National Polar-orbiting Operational Environmental Satellite System environmental data records," in *Weather and Environmental Satellites*, T. H. Vonder Haar and H.- L. Huang, eds., Proc. SPIE **5549,** 53–59 (2004).
23. W. Wiscombe, "The delta-M method: rapid yet accurate radiative flux calculations for strongly asymmetric phase functions," J. Atmos. Sci. **34,** 1408–1422 (1977).